CHAPTER 3

EXPERIMENTAL PROCEDURES

In this chapter, the experimental procedures employed for preparation and characterization of powders and ceramics of all systems will be described. Phase formation characterization and microstructure have been investigated using X-ray diffraction (XRD) and scanning electron microscopy (SEM), respectively. Electrical, mechanical and ferroelectric properties were also characterized. The details are presented in the following sections.

3.1 Sample preparation

Fabrication of the studied samples, BNZ and BNZT systems, was divided into two sections including powder preparation and ceramic fabrication. The detail is explained in each section.

3.1.1 Powder preparation

In this research, all powders have been synthesized by a solid-state mixed oxide method. All commercially starting compounds used to prepare the samples, suppliers, formula weights and purities of the materials are listed in Table 3.1.

Table 3.1 Specifications of the starting materials used in this study.

Powder	Source	Formula weight	Purity (%)
Bi_2O_3	Fluka	465.96	98%
Na_2CO_3	Riedel-de Haën	105.98	99.5%
ZrO_2	Riedel-de Haën	123.22	99%
TiO_2	Riedel-de Haën	79.87	99%

3.1.1.1 BNZ system

In powder synthesis of this system, the compound was prepared according to a chemical formula $Bi_{0.5}Na_{0.5}ZrO_3$. The BNZ powder was synthesized by a solid-state mixed oxide method. The following reaction was proposed for the formation of BNZ powder.

$$0.25Bi_2O_3 + 0.25Na_2CO_3 + ZrO_2 \longrightarrow (Bi_{0.5}Na_{0.5})ZrO_3 + 0.25CO_2 \quad (3.1)$$

For mixing process, the starting oxide powders which are Bi_2O_3, Na_2CO_3 and ZrO_2 were weighted following the calculated relevant proportions of constituents and were mixed in ethanol with zirconia media for 24 hours. After that, the mixed powder was dried employing the sample dish placed on a hotplate with the magnetic stirring in action to prevent gravitational separation of the components for 2 hours. Next, the dried powder was ground and calcined at different temperatures including 700, 750, 800 and 850°C for dwell times 2 hours with heating/cooling rate of 5°C/min in closed alumina crucible as shown in Fig. 3.1. A schematic diagram of the BNZ powder preparation is illustrated in Fig. 3.2.

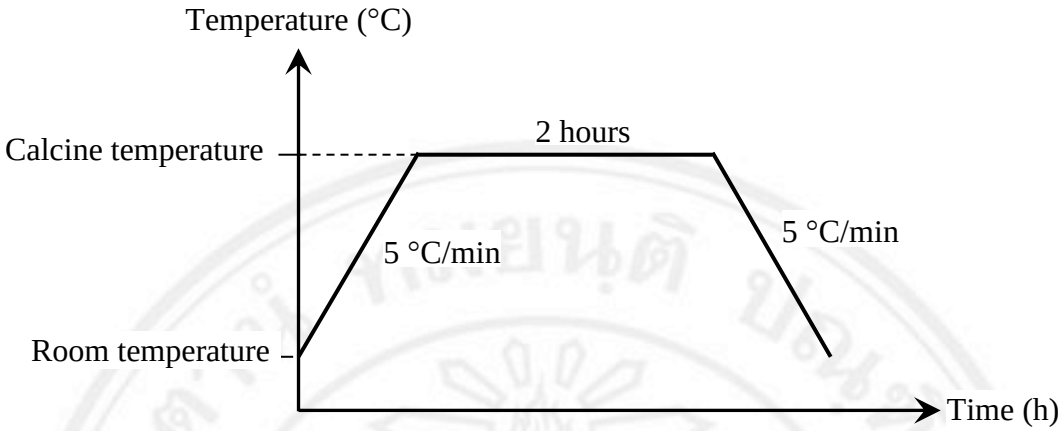

Figure 3.1 Diagram of calcination $Bi_{0.5}Na_{0.5}ZrO_3$ powder at different temperatures.

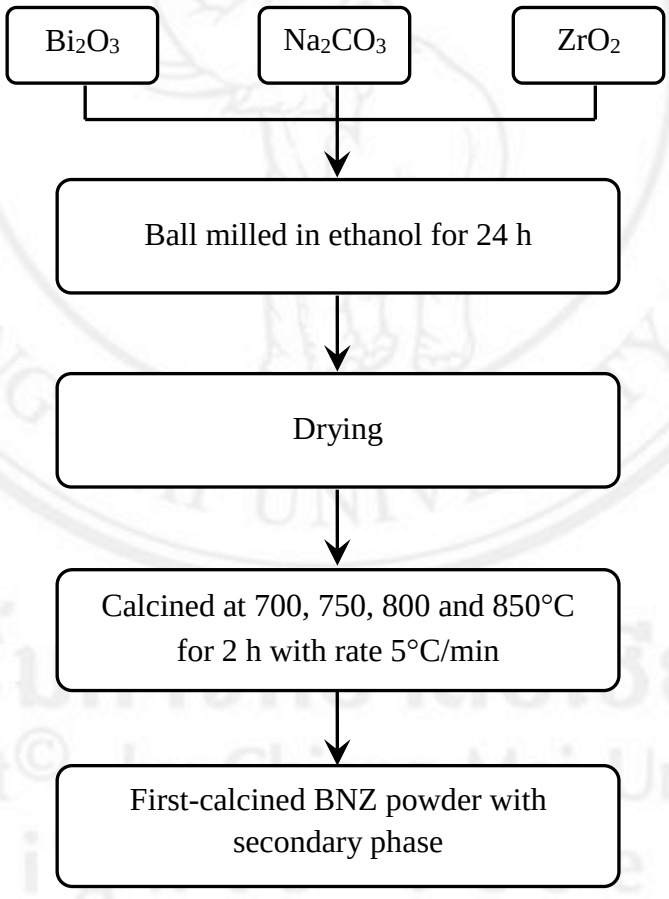

Figure 3.2 Diagram showing processing sequence of $Bi_{0.5}Na_{0.5}ZrO_3$ powders.

After first calcination, a secondary phase of starting powder that are Bi_2O_3 and ZrO_2 was found in the calcined powder. It was possible that the amount of some starting constituents was insufficient during BNZ crystallization. Therefore, the first-calcined powder was added separately in starting material content of 5, 10 and 15 wt% (namely BNZ/Bi_2O_3, BNZ/Na_2CO_3 and BNZ/ZrO_2) to help complete the chemical reaction during calcination at high temperature. Then, the starting material-modified powder was mixed again using mixed oxide method for 6 hours. The mixed powder was dried and ground again by the techniques similar to the above-mentioned procedure. Subsequently, the calcination of the powder was carried out again at 800°C for dwell time of 2 hours with a heating/cooling rate of 5°C/min in closed alumina crucible. This preparation condition showed minimized contamination of secondary phase. A schematic diagram of the addition of starting powder in BNZ powder preparation is illustrated in Fig. 3.3. The X-ray diffraction analysis was employed to identify the phases present in order to check the formation of BNZ powder with different starting powder conditions.

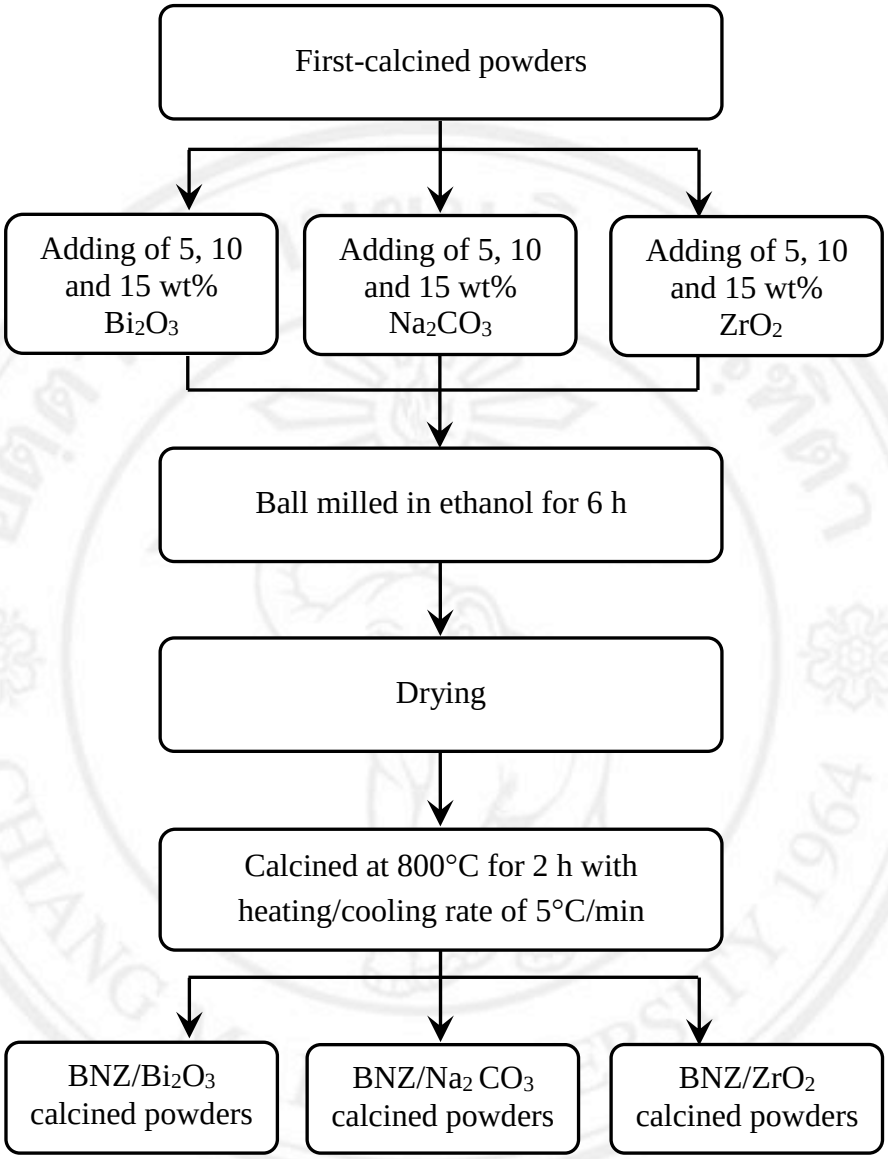

Figure 3.3 Diagram showing processing sequence of $Bi_{0.5}Na_{0.5}ZrO_3$ powder with addition of starting powders.

Effect of calcination time on formation of BNZ crystalline powder was also investigated in this work. The starting oxide powders which are Bi_2O_3, Na_2CO_3 and ZrO_2 were weighted following the calculated relevant proportions of constituents and were mixed in ethanol with zirconia media for 24 hours. After that, the mixed powder was dried. Next, the dried powder was ground and calcined at 800°C for various

dwell time, i.e. 2, 4 and 6 hours with a heating/cooling rate of 5°C/min in closed alumina crucible as shown in Fig. 3.4. A schematic diagram of the BNZ powder preparation is illustrated in Fig. 3.5. The X-ray diffraction analysis was employed to identify the phases in order to check formation of BNZ powder with different calcination time.

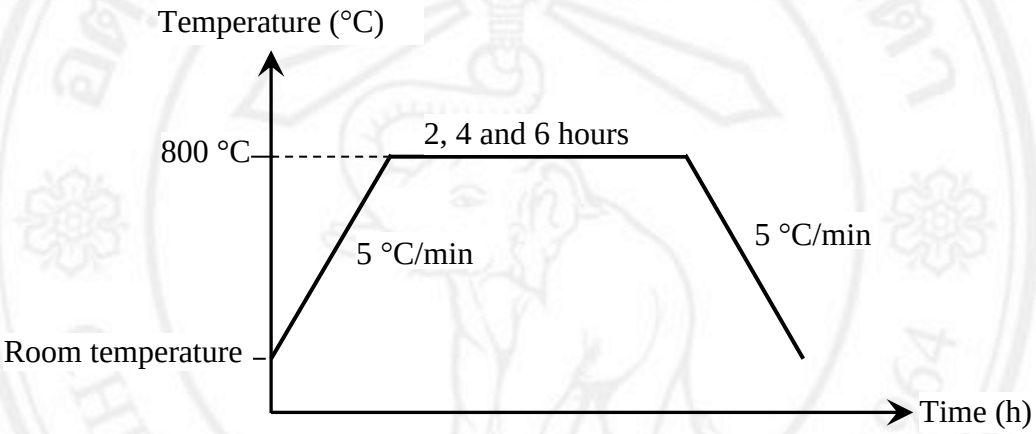

Figure 3.4 Diagram of calcination $Bi_{0.5}Na_{0.5}ZrO_3$ powder at different times.

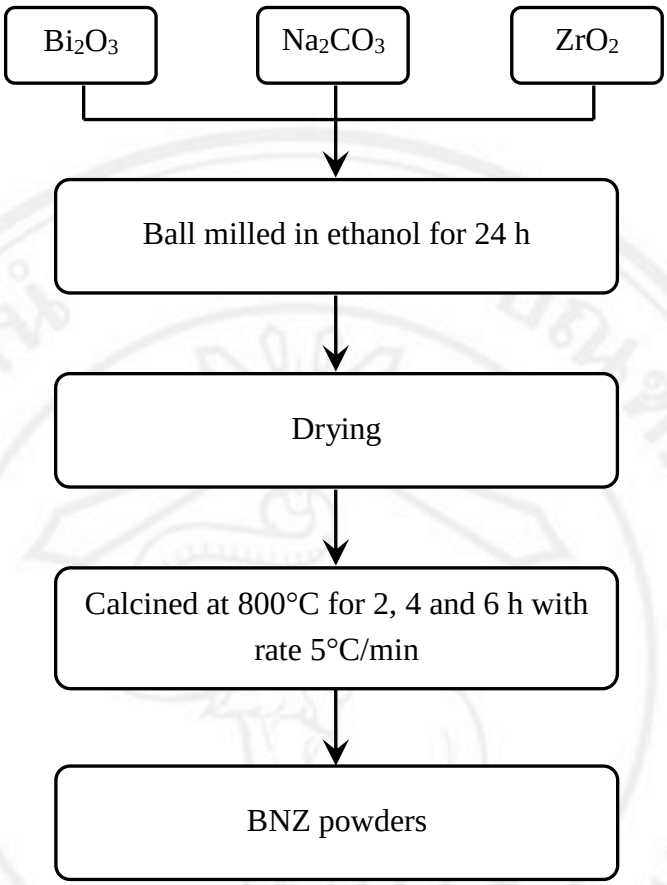

Figure 3.5 Diagram showing processing sequence of $Bi_{0.5}Na_{0.5}ZrO_3$ powders with different calcination times.

3.1.1.2 BNZT system

In this system, the powders were prepared by solid-state mixed oxide method with chemical formula $Bi_{0.5}Na_{0.5}Zr_{1-x}Ti_xO_3$ where x = 0.1, 0.2, 0.3, 0.4, 0.5 and 0.6 mole fraction. The starting chemicals used were Bi_2O_3, Na_2CO_3, ZrO_2 and TiO_2. The following reaction was proposed for the formation of BNZT powders:

$$Bi_2O_3 + Na_2CO_3 + (1\text{-}x)ZrO_2 + xTiO_2 \longrightarrow Bi_{0.5}Na_{0.5}Zr_{1-x}Ti_xO_3 + CO_2 \quad (3.2)$$

The starting powders were weighted, ball-milled and dried. The mixed powders were calcined at temperatures of 800 °C for dwell time of 2 hours with a

heating/cooling rate of 5°C/min in a closed alumina crucible. Figure 3.6 shows the calcination process of powders. The X-ray diffraction analysis was employed to identify the phase formation in order to check formation of BNZT powder. Figure 3.7 shows processing sequence of BNZT powder.

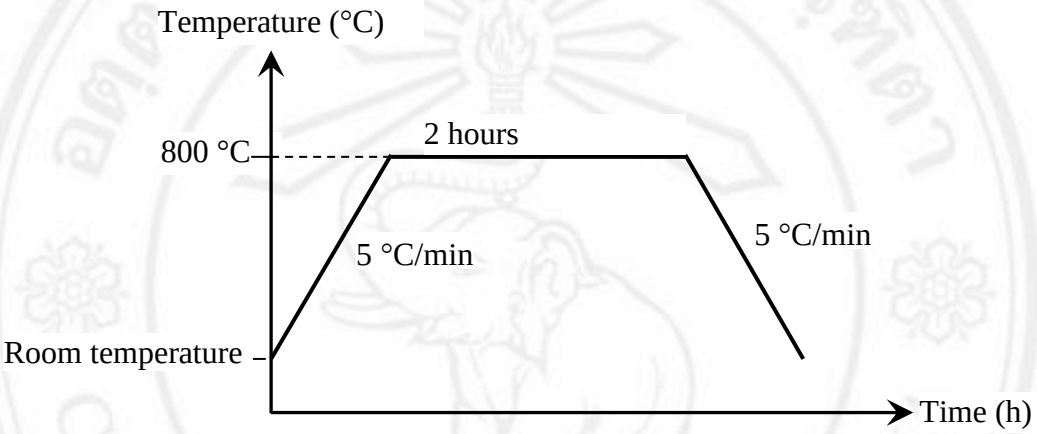

Figure 3.6 Diagram of calcination $Bi_{0.5}Na_{0.5}Zr_{1-x}Ti_xO_3$ powders.

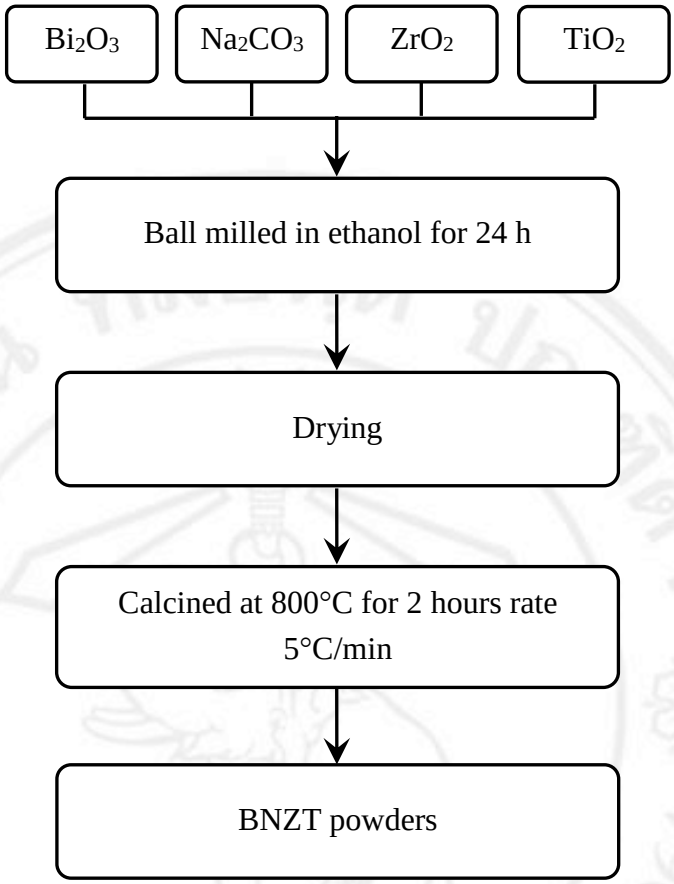

Figure 3.7 Diagram showing processing sequence of $Bi_{0.5}Na_{0.5}Zr_{1-x}Ti_xO_3$ powders.

3.1.2 Ceramic fabrication

In this section, ceramic fabrication of all systems has been carried out using a conventional sintering techniques i.e. solid-state sintering with and without sintering aids. The preparation of each ceramic system was discussed in the detail.

3.1.2.1 BNZ system

After obtaining the powder of this lead-free system, the solid state sintering technique with and without sintering aids were used to prepare ceramics. Fabrication of samples was explained in the following sections.

3.1.2.1.1 Solid state sintering

In this sintering technique, the BNZ powder was mixed with 3 wt% polyvinyl alcohol (PVA) used as a binder and was uniaxially pressed (0.6 g per batch) into a green pellet with a diameter of 10 mm. Then, the pellets were placed on a closed alumina plate. Figure 3.8(a) and (b) present the specimen arrangement with top and side view, respectively. As for firing process, the pellets were sintered at various temperatures of 850, 900, 950, 1000, 1050 and 1100°C in air for dwell time of 2 hours with a heating/cooling rate of 5°C/min. The sintering procedure is displayed in Fig. 3.9. Also, the whole processing sequence for the preparation of BNZ ceramics with different sintering temperatures is shown in Fig. 3.10.

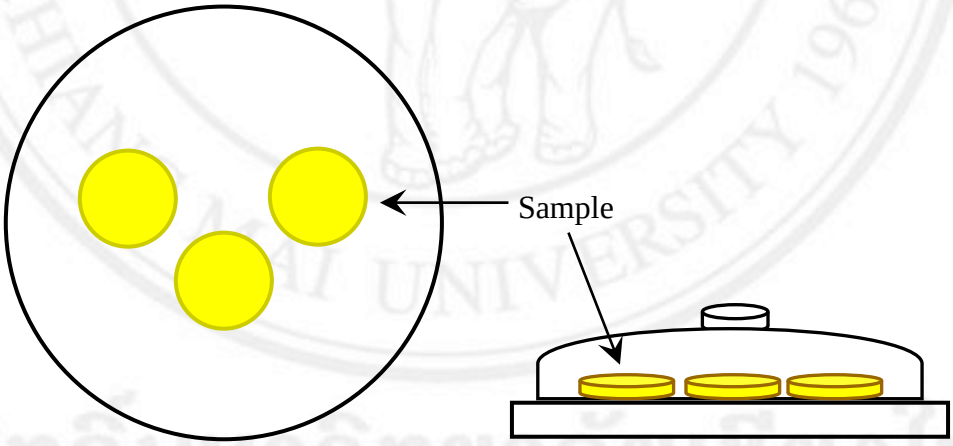

Figure 3.8 Sample arrangement for the sintering process where a = top view and b = side view.

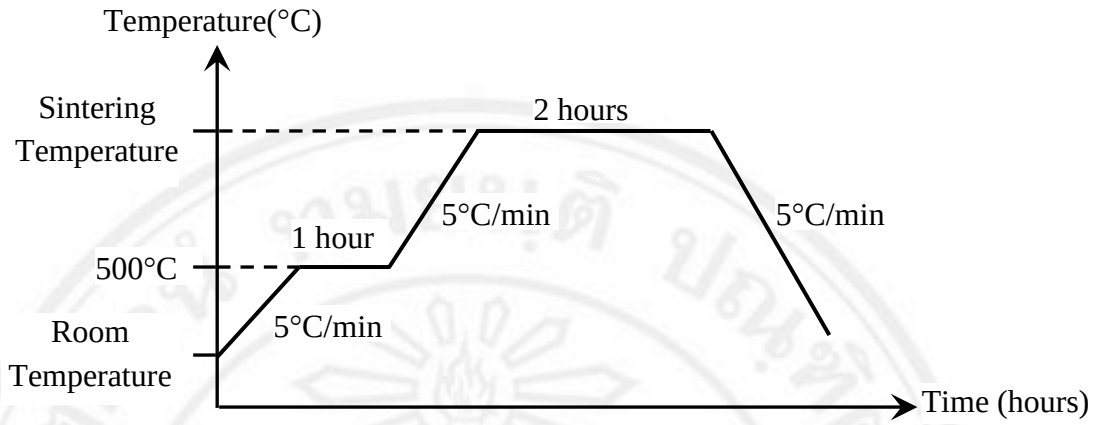

Figure 3.9 Diagram for sintering process of $Bi_{0.5}Na_{0.5}ZrO_3$ ceramic with different temperatures.

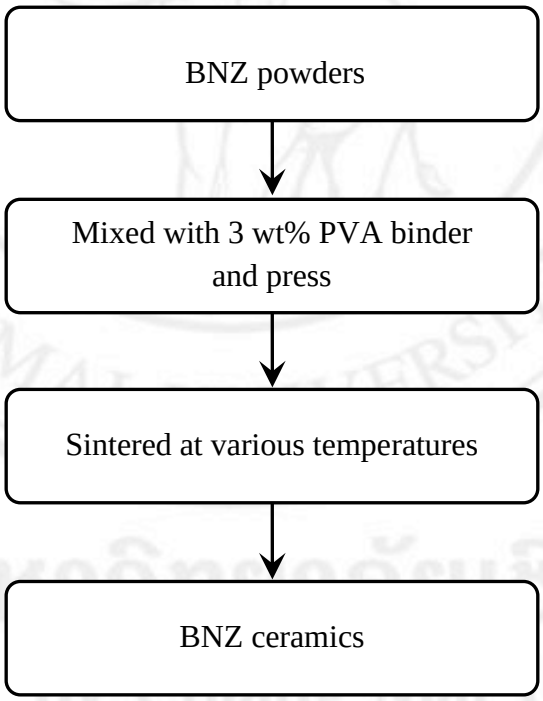

Figure 3.10 Diagram showing processing sequence of $Bi_{0.5}Na_{0.5}ZrO_3$ ceramic with different temperatures.

According to the result of BNZ fabrication at different temperatures, the sintering at 900°C was the optimized condition. Effect of sintering time was subsequently investigated. For the preparation, BNZ powder was mixed with 3 wt% polyvinyl alcohol (PVA) as a binder and was uniaxially pressed (0.6 g per batch) into a green pellet with a diameter of 10 mm. Then, the pellets were placed on a closed alumina plate liking that of previous fabrication procedure. For firing process, the pellets were sintered at 900°C in air for dwell time of 2, 4, 6 and 8 hours with a heating/cooling rate of 5°C/min. The sintering procedure is displayed in Fig. 3.11. Also, the whole processing sequence for the preparation of BNZ ceramics with time differences is shown in Fig. 3.12.

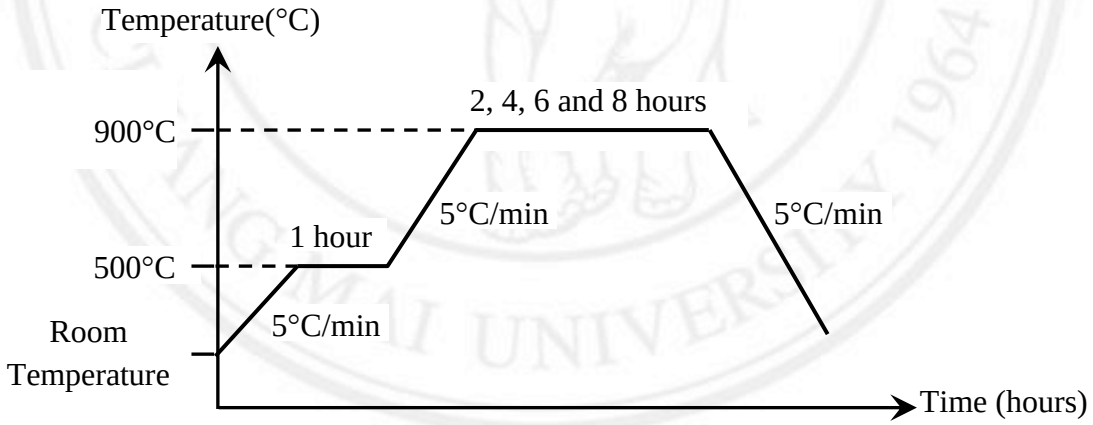

Figure 3.11 Diagram for sintering process of $Bi_{0.5}Na_{0.5}ZrO_3$ ceramic with different sintering times.

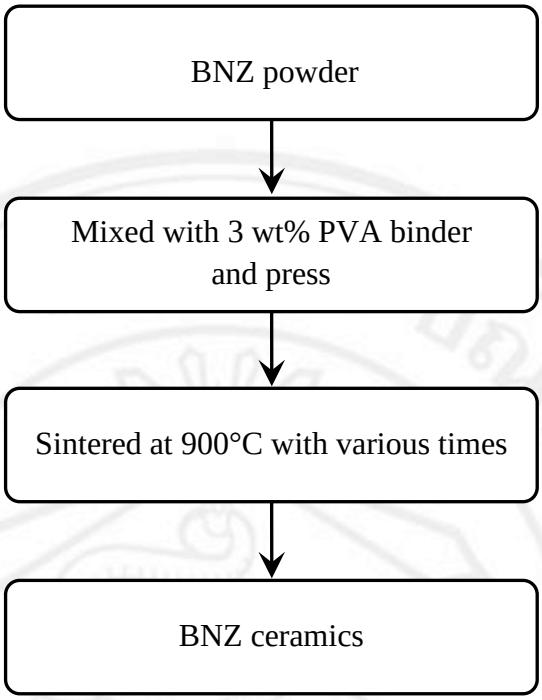

Figure 3.12 Diagram showing processing sequence of $Bi_{0.5}Na_{0.5}ZrO_3$ ceramic with different sintering times.

Investigation of BNZ powders with different ball milling times was also carried out in this study since it was believed that this could affect densification of this ceramic system. The calcined powders were ball milled again for 24, 48, 72 and 96 hours and then were dried. For the pellet preparation, the modified powder was mixed with 3 wt% polyvinyl alcohol (PVA) as a binder and was uniaxially pressed (0.6 g per batch) with a diameter of 10 mm. Then, the pellets were placed on a closed alumina plate liking that of previous fabrication procedure. For firing process, the pellets were sintered at 900°C in air for dwell time of 2 hours with a heating/cooling rate of 5°C/min. The sintering procedure is displayed in Fig. 3.13. Also, the whole processing sequence for the preparation of BNZ ceramics with different ball-milling time is shown in Fig. 3.14.

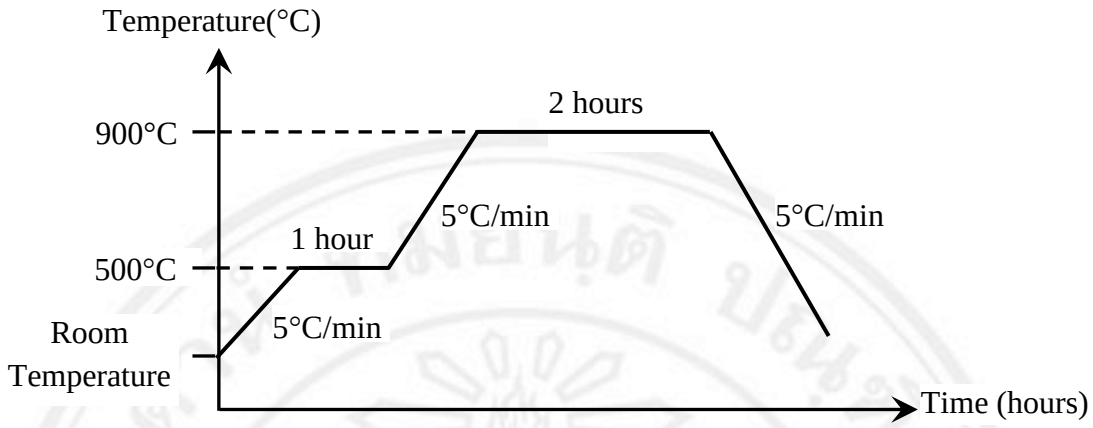

Figure 3.13 Diagram for sintering process of $Bi_{0.5}Na_{0.5}ZrO_3$ ceramic with different ball milling times.

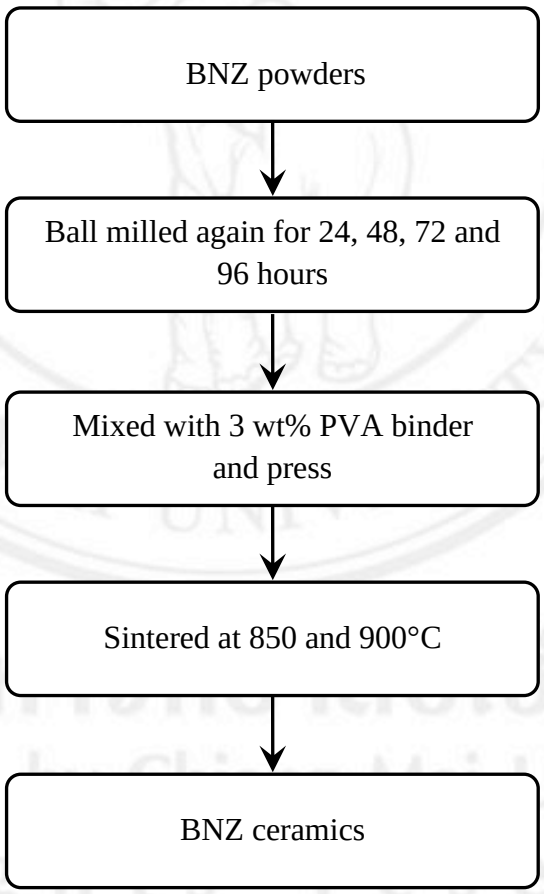

Figure 3.14 Diagram showing processing sequence of $Bi_{0.5}Na_{0.5}ZrO_3$ ceramic with different ball milling times.

3.1.2.1.2 Sintering aids

For BNZ fabrication using typical solid state sintering technique, the density of sintered samples was rather low. Hence, Bi_2O_3 and Na_2CO_3 as sintering aid were used to enhance densification of this ceramic system. Form previous study of ball milling time, the optimized condition was BNZ powder ground for 72 hours. Accordingly, the powder with this ball milling time was mixed with either Bi_2O_3 or Na_2CO_3 powder in concentration of 1, 4, 7 and 10 wt% for 6 hours. Then, the mixed powder was dried. For the pellet preparation, the doped powder was mixed with 3 wt% polyvinyl alcohol (PVA) as a binder and was uniaxially pressed (0.6 g per batch) with a diameter of 10 mm. Next, the pellets were placed on a closed alumina plate liking that of previous fabrication. For firing process, the pellets were sintered at 800, 850 and 900°C in air for dwell time of 2 hours with a heating/cooling rate of 5°C/min. The sintering procedure is displayed in Fig. 3.15. Also, the whole processing sequence for the preparation of BNZ ceramics using Bi_2O_3 or Na_2CO_3 as sintering aid is shown in Fig. 3.16.

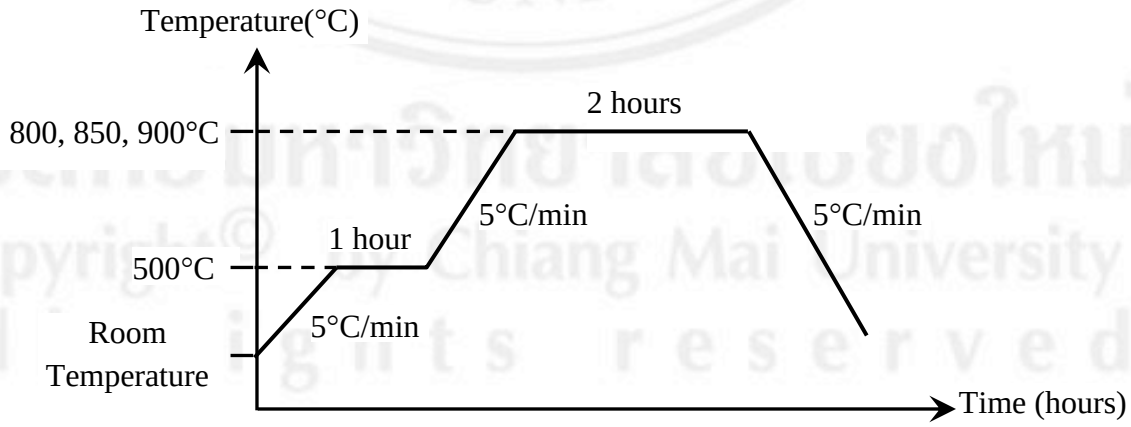

Figure 3.15 Diagram for sintering process of $Bi_{0.5}Na_{0.5}ZrO_3$ ceramic with Bi_2O_3 or Na_2CO_3 as sintering aids.

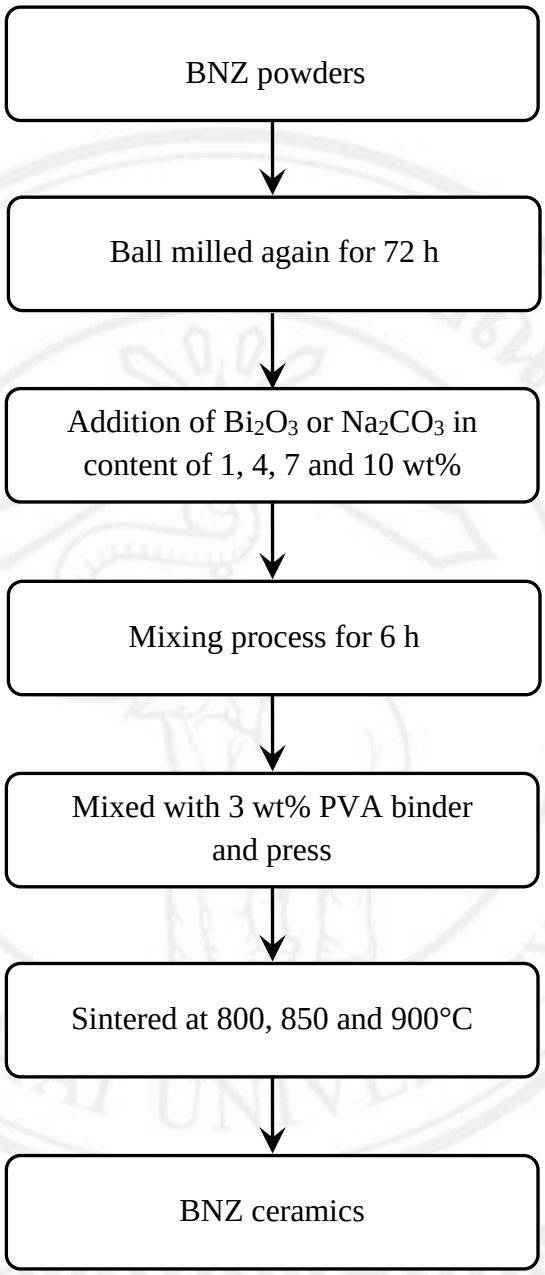

Figure 3.16 Diagram showing processing sequence of $Bi_{0.5}Na_{0.5}ZrO_3$ ceramic using Bi_2O_3 or Na_2CO_3 as sintering aids.

3.1.2.2 BNZT system

After obtaining the $Bi_{0.5}Na_{0.5}Zr_{1-x}Ti_xO_3$ powders, the mixed powders of each composition were uniaxially pressed (0.6 g per batch) into a green pellet with a diameter of 10 mm and 3 wt% polyvinyl alcohol (PVA) added as a binder. Following binder burn out at 500°C, the pellets were placed on the closed alumina plate. The specimen arrangement was not different from that of BNZ system shown in Figure 3.8. The pellets were sintered at sintering temperatures of 900 and 950°C in air for dwell time of 2 hours with a heating/cooling rate of 5°C/min, as shown diagramatically in Fig. 3.17. The whole processing sequence for the preparation of $Bi_{0.5}Na_{0.5}Zr_{1-x}Ti_xO_3$ ceramics is shown in Fig. 3.18.

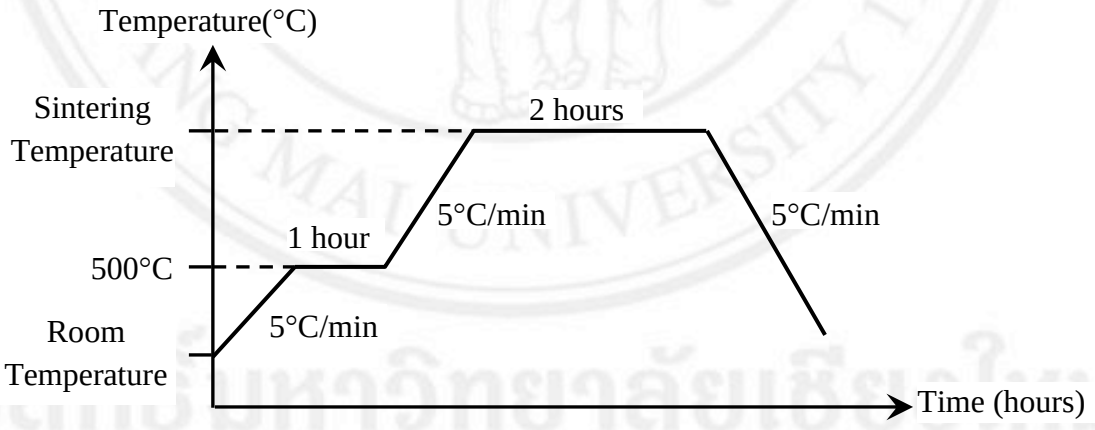

Figure 3.17 Diagram for sintering process of $Bi_{0.5}Na_{0.5}Zr_{1-x}Ti_xO_3$ ceramics.

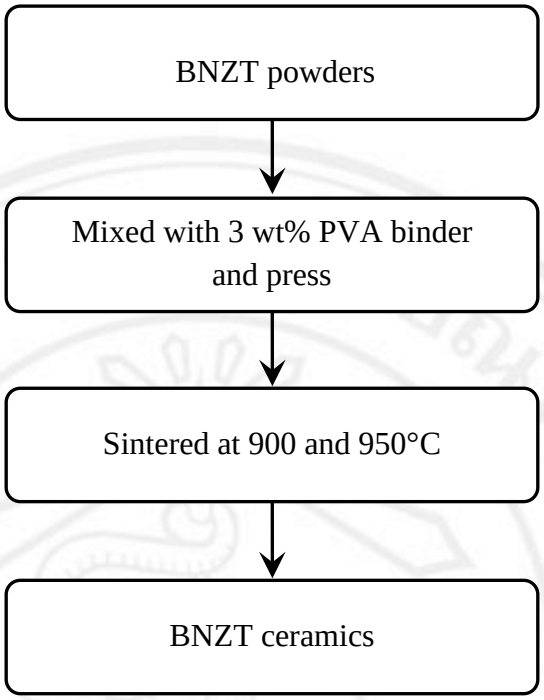

Figure 3.18 Diagram showing processing sequence of $Bi_{0.5}Na_{0.5}Zr_{1-x}Ti_xO_3$ ceramics.

3.2 Sample characterization

Characterization techniques used for subsequent investigation of phase formation, crystal structure, microstructures, dielectric and ferroelectric properties are described in the following section.

3.2.1 Thermal analysis

Thermal decomposition and weight loss behavior of the uncalcined powders was analyzed by differential scanning analysis (DSC) and thermogravimetric analysis (TGA), respectively. In this experiment, a differential scanning calorimeter (NETZSCH STA 409 PC/PG) shown in Fig. 3.19 was employed with platinum crucible, reference powder of Al_2O_3 and a heating rate of 10°C/min. The decomposition temperature and weight loss were recorded when the samples were heated from room temperature to 1350°C.

Figure 3.19 Q10 Differential scanning calorimeter.

3.2.2 Phase analysis

In this study, the optimum firing temperatures, phase analysis of mixed powders and sintered ceramics were carried out using an X-ray diffractometer (XRD); Phillips Model X-pert MPD (Fig. 3.20). The source of X-ray employed CuKα radiation of wavelength 1.5405 Å, with a tube voltage and current of 40 kV and 35 mA, respectively. Room temperature XRD data was recorded between 2θ from 20° to 90° with a step size of 0.02°/second.

Figure 3.20 X-ray diffractometer (Model Phillips Expert).

The X-ray beam incident on a material is partly scattered, absorbed and transmitted. The scattering of X-ray is related to the interaction between X-ray and crystal lattice of the materials. The X-ray scattered from different lattices interfere with each other and produces a diffraction pattern upon the change of incident angle

of the X-ray beam. The X-ray diffraction measurement configuration consists of the incident beam impinging on the sample material on a flat substrate and the X-ray diffracted at the same angle as the incident radiation is detected. Peak intensity will appear when Bragg's Law is satisfied as shown in Fig. 3.21. The corresponding Bragg's equation is

$$2d \sin\theta = n\lambda \tag{3.3}$$

where d is the interplanar spacing of the crystal,

θ is the angle of an incidence,

n is the integer order of the diffraction peak,

λ is the wavelength of the radiation (1.5405 Å).

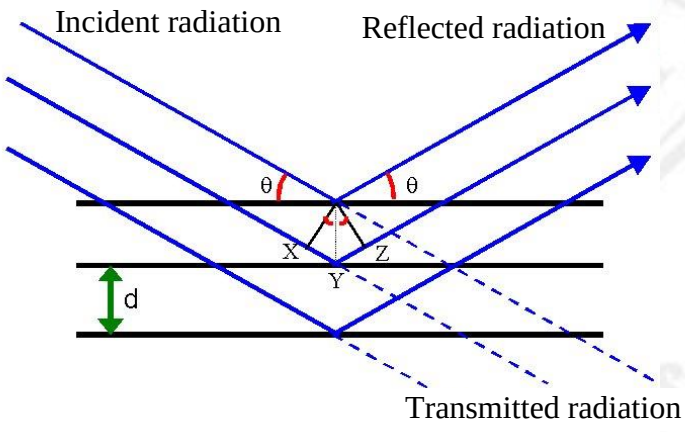

Figure 3.21 Schematic diagram of Bragg's law reflection.

3.2.3 Crystal structure analysis

In this work, crystal structure of the specimen was investigated using Powder Cell Software. The program introduced by W. Kraus and G. Nolze [33] was used to identify the crystal structure of the samples. Firstly, the important data of crystal structure (lattice parameters, crystal system and atom position) was the input of the program. The mentioned parameters could be varied. After that, the program generated a simulated pattern dependent on the given data. The software screen, the simulated pattern and a prototype unit cell created from the crystal data are presented in Fig. 3.22. Experimental XRD pattern was compared with the simulated pattern until the difference was minimized.

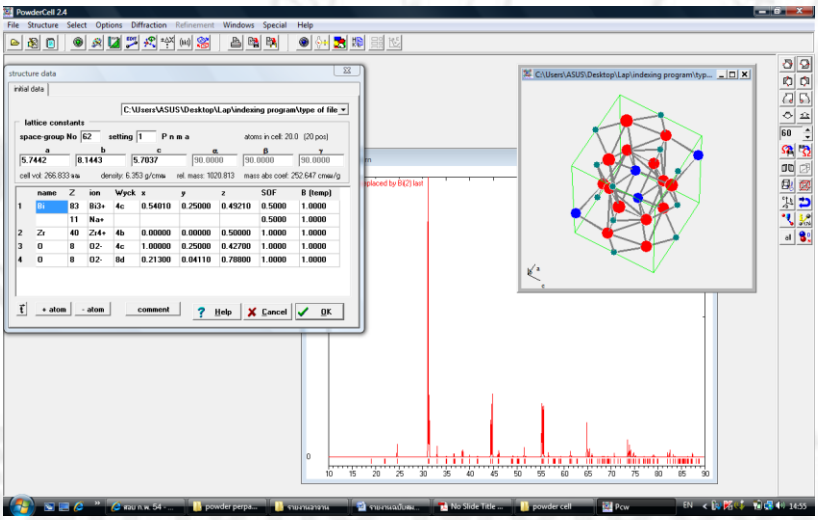

Figure 3.22 Feature of Powder Cell software.

3.2.4 Densification analysis

In this study, the bulk densities of sintered ceramics were determined using the Archimedes' principle. The sample is first weighed dry (w_1), then weighed again after fluid impregnation (w_2), and finally weighed while being immersed in fluid (w_3). The density (ρ) can be calculated from the following equation:

$$\rho = \frac{\rho_w w_1}{w_3 - w_2} \tag{3.4}$$

where ρ_w is the density of water (in g/cm^3), which is slightly temperature dependent, i.e.

$$\rho_w = 1.0017 - 0.0002315\,T \tag{3.5}$$

where T is the temperature of water (°C).

3.2.5 Microstructural analysis

In this work, the scanning electron microscope (SEM, JEOL JSM-6335F) as shown in Fig. 3.23, was used to determine the morphology of the powder, the surface and fracture area of the ceramics. The samples were polished and thermally etched at temperature of 150°C lower than the sintering temperature with a heating/cooling rate of 5°C/min for dwell time 15 minutes. The thermally etched surface and fracture surface of the ceramics were cleaned by ultrasonic cleaner and gold coated with sputtering coater (shown in Fig. 3.24). The range of grain size and average grain size were determined by using the linear intercept method on the SEM micrographs.

Figure 3.23 Scanning electron microscope (SEM, JEOL JSM-6335F).

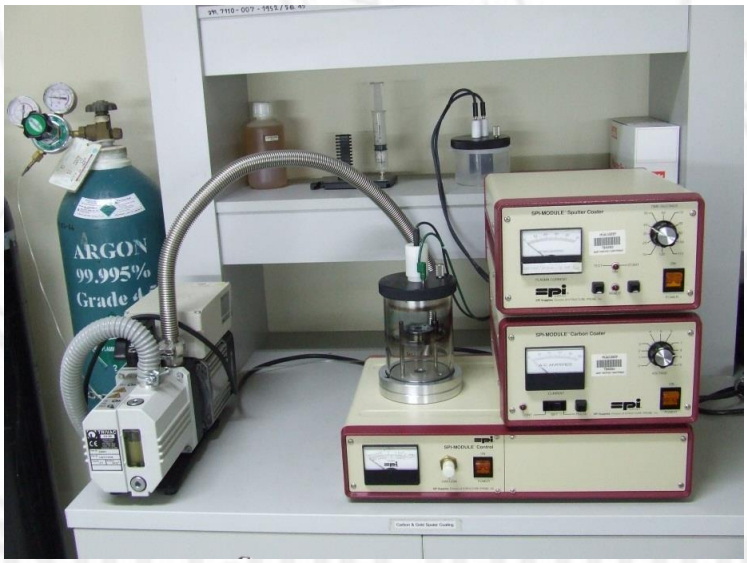

Figure 3.24 Sputter coater (JFC-1100E).

3.2.6 Mechanical property analysis

In this work, the studying of mechanical properties was carried out specially BNZ system. The measurement was indentation i.e. Vickers and Knoop hardness. The detail was explained in the section.

3.2.6.1 Vickers hardness

The digital microhardness tester (STARTECH, SMV-1000) with Vickers-type indenter as shown in Fig. 3.25, was used to measure the hardness of the BNZ and BNZT ceramics. For sample preparation, the specimens were polished into a diameter of 10 mm. The Vickers hardness value (*HV*) was calculated by the following equation:

$$HV = \frac{(1.854)P}{d^2} \tag{3.6}$$

where P is load applied to indenter (N),

d is the average length of the diagonal left by the indenter (μm).

Figure 3.25 Digital Microhardness Tester.

3.2.6.2 Knoop hardness

The above-mentioned instrument (STARTECH, SMV-1000) with Knoops-type indenter was also used to measure the hardness of the BNZ and BNZT ceramics. For sample preparation, it was not different from that of Vickers hardness measurement. The Knoops hardness value (*HK*) was calculated by the following equation:

$$HK = \frac{(14.23)P}{d^2} \tag{3.7}$$

where P is load applied to indenter (N),

d is the average length of the diagonal left by the indenter (μm).

Also, Young's modulus and fracture toughness of BNZ ceramics were calculated from the data of Vickers and Knoops measurement.

$$E = \alpha HK\left(\frac{b}{a} - \frac{b'}{a'}\right)^{-1} \tag{3.8}$$

where E is Young's modulus (GPa),

α is constant value of Marshall et al. (≈ 0.45),

HK is Knoop hardness (GPa),

b/a is ratio of the length of short diagonal per the length of long diagonal by the indenter (≈ 0.14),

b'/a' is ratio of the length of short diagonal per the length of long diagonal.

$$K_{IC} = 0.016\left(\frac{E}{HV}\right)^{1/2}\left(\frac{P}{c^{3/2}}\right) \quad (3.9)$$

where K_{IC} is Fracture toughness (MPa.m$^{1/2}$),

E is Young's modulus (GPa),

HV is Vickers hardness (GPa),

P is applied load (N),

c is the crack length for edge crack and center of indentation (m).

3.2.7 Thermal expansion property analysis

In case of thermal expansion measurements, all samples were cut in bar shape (5 mm long and 1 mm^2 cross-section), placed inside a fused silica holder, heated at a rate of 2^{o}C/min from -100 to 500^{o}C and the thermal expansion was measured as a function of temperature using a linear voltage-differential transformer (LVDT) dilatometer as shown in Fig 3.26. The LVDT has an advantage over other transformers as it gives a linear output for every unit displacement. The thermal expansion coefficient (α) and thermal strain (ε) was calculated by Eq. 3.10 and 3.11, respectively.

$$\alpha = \frac{(L_{final} - L_{initial})}{L_{initial}(T_{final} - T_{initial})} \quad (3.10)$$

$$\varepsilon = \frac{L_{final} - L_{initial}}{L_{initial}} \quad (3.11)$$

where $L_{initial}$ is initial length of the sample (mm),

L_{final} is final length of the sample (mm),

$T_{initial}$ is initial temperature (^{o}C),

T_{final} is final temperature (^{o}C),

Figure 3.26 The thermal expansion measurement.

3.2.8 Dielectric property analysis

For dielectric measurement, the sintered samples were lapped to obtain parallel faces, which were subsequently coated with silver paint as electrodes. Then, the samples were tested with digital multimeter to check the quality of the electrodes. The dielectric properties were studied with an automated dielectric measurement system, LCZ-meter (Hewlett Packard 4194A) as shown in Fig. 3.27 for room temperature and in Fig. 3.28 for different temperatures. The capacitance and the dielectric loss tangent were determined at room temperature and several temperatures with the frequency of

1, 10 and 100 kHz. Therefore, the dielectric constant (ε_r) was then calculated by the following equation:

$$\varepsilon_r = \frac{Cd}{\varepsilon_0 A} \tag{3.12}$$

where C is the capacitance of the sample (F),

ε_0 is the dielectric permittivity of vacuum (8.854×10^{-12} F/m),

A is the area of the electrode of the sample (m^2),

d is the thickness of the sample (m).

Figure 3.27 The dielectric properties measurement at room temperature.

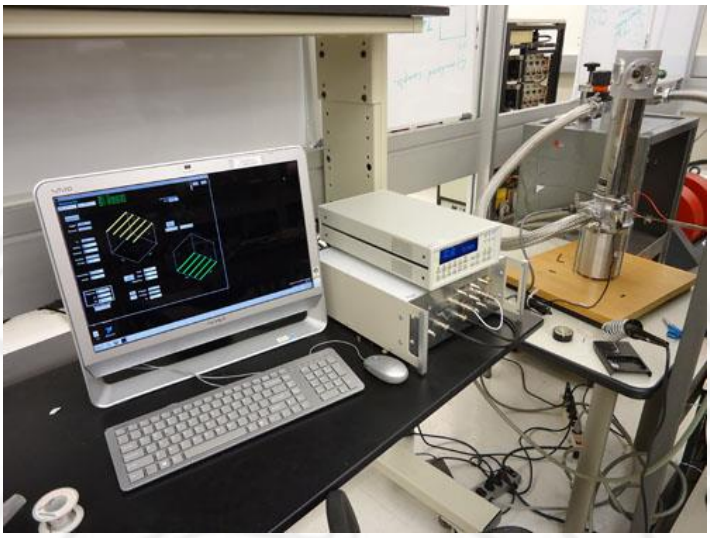

Figure 3.28 The dielectric properties measurement at different temperature.

3.2.9 Electrical conduction analysis

Initially, the samples were polished into a diameter of 1 cm. Then, the resistance of the studied pellets was measured employing 4-point linear probe with electrometer/high resistance meter (KEITHLEY, 6517A) as shown in Fig. 3.29. After obtaining the resistance parameters, a resistivity (ρ) can be calculated by Eqn. 3.13, which gives

$$R = \rho \frac{l}{A} \tag{3.13}$$

where R is resistance of the sample (Ω),

ρ is resistivity of the samples (Ω.m),

A is the area of the electrode of the sample (m^2),

l is the thickness of the sample (m).

Also, a conductivity of the samples can be obtained according to the inverse of that of resistivity as given in Eqn. 3.14:

$$\sigma = \frac{1}{\rho} \tag{3.14}$$

where σ is conductivity of the sample $(\Omega.m)^{-1}$ or $(S.m^{-1})$,

ρ is resistivity of the samples $(\Omega.m)$.

Figure 3.29 The resistivity and conductivity measurements.

3.2.10 Ferroelectric property analysis

The ferroelectric hysteresis (*P-E*) loops were characterized using a computer controlled modified Sawyer-Tower circuit. The electric field was applied to a sample by a high voltage AC amplifier (PDA 100) and transformer (Engicon) with the sinusoidal input signal at fixed measuring frequency of 50 Hz from a function generator (GAG-809). The *P-E* loops were recorded by a digital oscilloscope (Picotechnology 2204), as shown in Fig. 3.30. The system is an automated device intended primarily for measuring the polarization of materials induced by an electric field. From each measurement, the samples were then placed inside the sample holder, which was submerged in a silicone oil bath to prevent the electrical breakdown of the sample and then connected to the standard capacitor on Sawyer-Tower circuit. The sample could be considered as a capacitor (C_s) connected in series to the standard capacitor (C_0). Since the capacitance of the sample was much smaller than that of the standard capacitor, almost all of the electric potential of the high voltage source acts on the sample.

Figure 3.30 Ferroelectric hysteresis loop measurement.

By definition, polarization is the value of dipole moment per unit volume or amount of charge accumulated per unit surface area. Polarization of the sample induced by electric field loading, $P_{sample,}$ was given by

$$P_{sample} = \frac{Q_s}{A} \tag{3.15}$$

where Q_s is the amount of charges accumulated on the electrode of the sample (C),

A is the area of the electrode of the sample (cm^2).

Since the reference capacitor was connected in series to the sample, then amount of charges are equivalent:

$$Q_s = Q_0 \tag{3.16}$$

where Q_0 is the amount of charges accumulated on the standard capacitor (C).

On the other hand, the amount of charges on the standard capacitor is equal to:

$$Q_0 = V_y C_0 \tag{3.17}$$

where V_y is the voltage across the standard capacitor (V),

C_0 is the capacitance of the standard capacitor (= 1 µF).

Then, the polarization induced by electric field loading could be calculated as the following equation:

$$P_{sample} = \frac{V_y C_0}{A} \tag{3.18}$$

Consequently, by monitoring the voltage across the standard capacitor, the polarization of the sample could be determined.

From the x-axis of the monitor of oscilloscope, the electric field was calculated using the following equation:

$$E = \frac{V_x}{d} \tag{3.19}$$

where E is the electric field applied to the sample (V/cm),

V_x is the voltage across the circuit (V),

d is the thickness of the sample (cm).